TECHNIQUES AND RESOURCES

Chimeric 3D-gastruloids – a versatile tool for studies of mammalian peri-gastrulation development

Alexandra E. Wehmeyer[1], Katrin M. Schüle[1], Alexandra Conrad[1], Chiara M. Schröder[1,2,3,4], Simone Probst[1], and Sebastian J. Arnold[1,4]

[1]Institute of Experimental and Clinical Pharmacology and Toxicology, Faculty of Medicine, University of Freiburg, Albertstrasse 25, D-79104 Freiburg, Germany
[2]Spemann Graduate School of Biology and Medicine (SGBM), University of Freiburg, Albertstrasse 19a, D-79104 Freiburg, Germany
[3]Faculty of Biology, University of Freiburg, Schänzlestrasse 1, D-79104 Freiburg, Germany
[4]Signaling Research Centers BIOSS and CIBSS, University of Freiburg, Schänzlestrasse18, D-79104 Freiburg, Germany

For Correspondence: sebastian.arnold@pharmakol.uni-freiburg.de

ORCID Alexandra E. Wehmeyer 0000-0002-9981-8042
ORCID Katrin M. Schüle 0000-0001-6642-0030
ORCID Alexandra Conrad 0000-0001-7766-5033
ORCID Chiara M. Schröder 0000-0001-5345-3415
ORCID Simone Probst 0000-0002-0220-5400
ORCID Sebastian J. Arnold 0000-0002-2688-9210

Key words
Chimeric *3D*-Gastruloids, mESCs, *Eomes*, *Brachyury*, functional genetics, axis formation, cell lineage specification, Tbx transcription factors

Abstract

Stem cell-derived 3D-gastruloids show a remarkable capacity of self-organisation and recapitulate many aspects of gastrulation stage mammalian development. Gastruloids can be rapidly generated and offer several experimental advantages, such as scalability, observability, and accessibility for manipulation. Here, we present approaches to further expand the experimental potency of murine 3D-gastruloids by utilizing functional genetics in mouse embryonic stem cells (mESCs) to generate chimeric gastruloids. In chimeric gastruloids fluorescently labelled cells of different genotypes harbouring inducible gene-expression, or loss-of-function alleles, are combined with wildtype cells. We showcase this experimental approach in chimeric gastruloids of mESCs carrying homozygous deletions of the Tbx transcription factors *Brachyury,* or inducible expression of *Eomes.* Resulting chimeric gastruloids recapitulate reported *Eomes* and *Brachyury* functions, such as instructing cardiac fate and promoting posterior axial extension, respectively. Additionally, chimeric gastruloids revealed previously unrecognized phenotypes such as tissue sorting preference of *Brachyury*-deficient cells to endoderm, and cell non-autonomous effects of *Brachyury*-deficiency on *Wnt3a*-patterning along the embryonic axis, demonstrating some of the advantages of chimeric gastruloids as efficient tool for studies of mammalian gastrulation.

Introduction

The versatile experimental opportunities offered by functional genetics available in the mouse as main mammalian model system have greatly enhanced our understanding of embryonic development. However, studies of mammalian embryogenesis are hampered by the relative inaccessibility of the embryo due to intrauterine growth. *Ex vivo* embryo cultures partially overcome some of the experimental restrictions but rely on the isolation of often limiting numbers of embryos. More recently, novel approaches were developed to generate stem cell derived, 3D-embryoids reflecting different stages of mammalian development from the formation of the blastocyst (Kagawa et al., 2022; Li et al., 2019; Yu et al., 2021), to periimplantation embryos (Amadei et al., 2021; Harrison et al., 2017; Harrison et al., 2018), and postimplantation stages recapitulating early organogenesis (Beccari et al., 2018; Moris et al., 2020; Turner et al., 2017; van den Brink et al., 2020; van den Brink et al., 2014; Veenvliet et al., 2020). These embryoid models demonstrate the remarkable self-organisation and robustness of

embryonic programs that guide the processes of morphogenesis, growth, cell lineage specification and differentiation in the embryo as well as by *in vitro* models.

Among widely used embryoid model system are 3D-gastruloids, offering a simple experimental procedure to reproducibly generate embryoids that recapitulate development stages from early gastrulation to somitogenesis and onset of organogenesis (comparable to Embryonic days 6.5 (E6.5) – E9.0) reviewed in (van den Brink and van Oudenaarden, 2021; Veenvliet et al., 2021). 3D-gastruloids are formed by the aggregation of 100-300 mouse or human pluripotent embryonic stem cells (m or hESCs) that are treated by a 24 h pulse of the GSK3b-inhibitor CHIR to activate the canonical Wnt-cascade. This signalling stimulus induces an anterior-posterior asymmetry in the aggregate (van den Brink et al., 2014), indicated by the one-sided expression of the Tbx factor *Brachyury* that in the embryo marks the site of primitive streak formation at gastrulation onset (Rivera-Perez and Magnuson, 2005; reviewed in Arnold and Robertson, 2009). The *Brachyury*-expressing posterior pole of 3D-gastruloids elongates over several days thereby forming different tissues resembling paraxial mesoderm, neural tube, and the primitive gut tube. 3D-gastruloids show a remarkable self-organizing capacity as the different tissues are generated in proper spatial organization and arranged according to the embryonic axes (Beccari et al., 2018). 3D-gastruloids thus can be used as model systems for studies of various gastrulation-associated morphogenetic processes, as exemplified for somitogenesis (van den Brink et al., 2020; Veenvliet et al., 2020). However, some tissues of gastrulation stage embryos are less represented in 3D-organoids, including anterior mesoderm derivatives, such as cardiogenic mesoderm, and cranial structures such as cranial neural tissues (van den Brink et al., 2020; Veenvliet et al., 2020). This underrepresentation of anterior/cranial tissues most likely results from the initial induction of ESC aggregates with CHIR which imposes a strong signal for tissue identities of the posterior/caudal primitive streak (Dunty et al., 2008). However, this and other aberrations of 3D-gastruloids compared to embryos can also be used to investigate which additional regulatory requirements need to be met for proper morphogenesis of tissues and organ *anlagen* to more closely recapitulate the embryo (Veenvliet et al., 2021). Due to the scalability of this ESC- derived embryoid culture system, multiple different environmental cues can be readily tested. It is thus expected that further refinements of current protocols will lead to the generation of gastruloids

that more closely resemble the full spectrum of gastrulation and following stages of embryogenesis.

Cell specification to mesoderm and definitive endoderm (DE) cell lineages is regulated by two Tbx transcription factors *Eomesodermin* (*Eomes*) and *Brachyury (T)*. Functions of both factors were previously extensively studied in mouse establishing crucial roles of *Eomes* for cell lineage specification of definitive endoderm (DE) (Arnold et al., 2008; Teo et al., 2011) and anterior mesoderm (Costello et al., 2011), and functions of *Brachyury* for the generation of posterior mesoderm derivatives, and notochord (Wymeersch et al., 2021). The compound genetic deletion of *Eomes* and *Brachyury* completely abrogates specification of any ME during differentiation of pluripotent cells (Tosic et al., 2019). While functions of these Tbx factors for specification of cell fate are well described, their roles in tissue-wide morphogenetic processes are less defined. For example, the genetic deletion of *Eomes* in the epiblast abrogates formation of the mesoderm (and DE) cell layer, hindering studies of morphogenetic functions of *Eomes*-regulated programs (Arnold et al., 2008). Similarly, studies of the cell-intrinsic roles of *Brachyury* in posterior body axis extension are compromised by cell non-autonomous functions of *Brachyury* in feed-forward regulatory loops to maintain caudal Wnt-signals, that could independently act on cell specification and morphogenetic programs (Arnold et al., 2000; Dunty et al., 2008; Martin and Kimelman, 2008; Turner et al., 2014; Yamaguchi et al., 1999). These constraints to distinguish cell-autonomous effects of loss-of-gene-function from secondary effects, such as by general disturbance of morphogenesis, can be experimentally addressed by the generation of embryonic chimeras. Here, cell-autonomous gene functions can be studied when limited numbers of genetically altered cells are placed in an otherwise wildtype cellular environment. Chimeric approaches were previously reported for studies of *Brachyury* functions, such as in zebrafish (Halpern et al., 1993) and mouse (Wilson et al., 1993; Wilson et al., 1995; Wilson and Beddington, 1997), as well as for *Eomes* functions (Arnold et al., 2008), indicating regulatory roles of both Tbx factors in cell migration and morphogenesis. However, embryonic chimera analyses are highly labour and resource intensive, especially in mouse, and thus are only infrequently employed.

In this report, we demonstrate an approach to further increase the experimental potency of murine 3D-gastruloids by expanding it to chimeric analyses. We use genetically engineered, traceable mESCs to generate chimeric 3D-gastruloids that are

134 composed of cells with different genotypes. To showcase the advantages of this
135 approach and to test experimental feasibility we generated fluorescently labelled
136 mESC lines with homozygous loss-of-function, or inducible expression cassettes for
137 the two Tbx transcription factors *Brachyury* and *Eomes*. These are used to generate
138 chimeric gastruloids, e.g. by mixing defined ratios of inducible Tbx-expressing, or Tbx-
139 deficient and WT cells to generate chimeric situations with defined cell contribution that
140 are normally only difficult to achieve by conventional genetic tools or by cell injections
141 into embryos. In addition to demonstrating the efficiency and feasibility of this
142 experimental approach of chimeric gastruloids, this study also provides some
143 previously unrecognized insights into the morphogenetic functions of *Eomes* and
144 *Brachyury.*
145
146 **Results and Discussion**
147 To expand the experimental versatility of the 3D-gastruloid model system we combined
148 it with the use of genetically modified mESCs and fluorescent imaging. We generated
149 chimeric gastruloids composed of cells with different genetic backgrounds that can be
150 readily traced by different fluorescent membrane labels (Fig. 1A, B). WT mESCs are
151 permanently labelled by monoallelic knock-in of membrane GFP (mG) into the Rosa26
152 genomic locus (Fig. 1C), while membrane Tomato (mT) labelling was used for
153 genetically manipulated mESCs lines (Fig. 1C). Genetic alterations used in presented
154 experiments were the homozygous deletion of the Tbx transcription factor *Brachyury*
155 (*Bra*$^{-/-}$), and the ICE-mediated (induced cassette exchange) targeted integration of
156 *Eomes* 3' to a monoallelic Tet-responsive element (TRE) in A2lox (E14-based)
157 mESCs (Iacovino et al., 2014), resulting in TRE.*Eomes*GFP (short TRE.*Eo*). These
158 cell lines were first tested for their abilities to form regular gastruloids. This
159 demonstrated that fluorescent membrane labels don't have an impact on gastruloid
160 formation, while *Bra*$^{-/-}$ and dox-induced TRE.*Eo* cells show a failure to form regularly
161 extended gastruloids at 120 h (Supplementary Fig. 1). To generate chimeric
162 gastruloids we followed two approaches (Fig. 1A, D, E), either by mixing of different
163 cells during the aggregation of mESCs at the beginning of gastruloid culture (Fig. 1E),
164 or by merging of two preformed mESCs aggregates composed of different cells 24 h
165 after the initial aggregation (Fig. 1 B, D). Such merged ESC aggregates rapidly fuse
166 and stably adhere after placing them together in 96-wells (Fig. 1D, Supplementary
167 Movie 1) or in hanging drops (not shown).

168 The mixing of cells at different ratios can be used to evaluate cell-autonomous vs. cell
169 non-autonomous gene functions, by testing how different levels of cell contribution
170 affects tissue behaviour, e.g. when using cells with loss-of-gene-function. Merging of
171 cell aggregates can be applied when the behaviour of coherent groups of cells is
172 analysed, such as in studies of inductive tissue interactions. A similar approach was
173 recently reported where a small aggregate of 50 cells was treated with BMP4 to induce
174 organizer-activities which was used instead of CHIR-treatment for the induction of
175 gastruloid-formation (Xu et al., 2021). Thus, chimeric gastruloids offer multiple
176 experimental opportunities to study gastrulation development (Fig. 1A) as exemplarily
177 demonstrated in following experiments.
178 First, we tested if chimeric gastruloids are a suitable model to study instructive gene
179 functions during lineage specification. Hence, we generated chimeric gastruloids by
180 merging preformed aggregates of WT mESCs (mG-label) and mESCs containing the
181 doxycycline (Dox) inducible *Eomes*.GFP expression cassette (TRE.*Eo*; mT-label) (Fig.
182 2A, B). *Eome*s is crucially required for lineage specification towards definitive
183 endoderm (Arnold et al., 2008; Teo et al., 2011) and anterior mesoderm, including the
184 cardiac lineage (Costello et al., 2011; Probst et al., 2021). We tested if forced *Eomes*
185 expression in a group of cells (TRE.*Eo*) within a gastruloid would be sufficient to induce
186 a coherent heart-like domain, which is only inconsistently forming in gastruloids
187 composed of WT mESCs (Rossi et al., 2021; van den Brink and van Oudenaarden,
188 2021). Indeed, Dox-induced *EomesGFP*-expressing cells form a domain of beating
189 cardiomyocytes (Fig. 2C, Supplementary movie 2) in chimeric gastruloids in 33.7% (±
190 3.0 SD) of cases, whereas similar beating areas are only observed in 1.5% (± 2.5 SD)
191 in uninduced chimeric gastruloids (Fig. 2D) or using only A2lox WT mESCs (not
192 shown). To correlate induced *EomesGFP* expression with the cardiogenic domain we
193 performed *in situ* hybridization analyses for early cardiac markers *Mlc2a* and *Nkx2.5*,
194 which are expressed in mT-marked TRE.*Eo* cells that are forming a coherent domain
195 on one side of gastruloids (Fig. 2E, F). To analyse the position of TRE.*Eo* cell-derived
196 domains along the AP axis of merged chimeric gastruloids, we performed
197 immunostainings against BRACHYURY and CDX2, indicating the posterior pole of
198 extending gastruloids (Fig. 2G, H). The domains of TRE.*Eo* cells are predominantly
199 found on one side along the AP-axis of the gastruloids and oriented towards the
200 anterior pole (Fig. 2G, H). Of note, these coherent domains of cells are not found in
201 gastruloids when two preformed aggregates of WT cells are merged where cells

202 undergo increased mixing (Supplementary Fig. 2A). Interestingly, TRE.*Eo* cell
203 containing gastruloids consistently showed a reduction in axis extension, so that the
204 anterior-posterior (AP) axis of resulting gastruloids is less obvious in comparison to
205 only WT-derived gastruloids (Supplementary Fig. 2B, C). In short, these experiments
206 show that induced expression of *Eomes* suffices to cell-autonomously generate
207 coherent cardiogenic domains oriented to the anterior-lateral side of developing
208 gastruloids in a highly increased proportion of gastruloids compared to uninduced
209 gastruloids.
210 Next, we aimed for testing the feasibility of chimeric gastruloids for the assessment of
211 cell-autonomous vs. cell non-autonomous functions of *Brachyury* during posterior
212 elongation, as the shortening of the posterior body axis is the most prominent
213 phenotype of *Brachyury*-mutant embryos (Fig. 3A)(Wymeersch et al., 2021).
214 Gastruloids entirely generated from mT-labelled *Bra*$^{-/-}$ mESCs present with a
215 phenotype of impaired elongation, reminiscent of the failure of tailbud elongation
216 observed in *Brachyury*-mutant embryos (Fig. 3B, E; Supplementary Figs. 1, 3B) (Inman
217 and Downs, 2006). Increasing the proportional contribution of WT cells (mG) to the
218 gastruloid by intermixing WT with *Bra*$^{-/-}$ mESCs during the initial aggregation of 300
219 mESCs leads to the gradual extension and increase in overall tissue mass of the
220 posterior portion of the mixed gastruloids (Fig. 3B). We analysed BRACHYURY
221 presence in the WT cells in the posterior regions of chimeric gastruloids with high
222 (80%) and equal (50%) contribution of *Bra*$^{-/-}$ cells at 24 h time intervals. The posterior
223 region of chimeric gastruloids with a contribution of *Bra*$^{-/-}$ cells of 80% show less
224 confined and reduced a-BRACHYURY staining (Fig. 3C) compared to chimeric
225 gastruloids where *Bra*$^{-/-}$ cell contribution is 50%. Here, *Brachyury* expression is found
226 robustly but with decreased intensity in the posterior pole when compared to WT
227 gastruloids (Fig. 3D, and Supplementary Fig. 3A).
228 The absence of *Brachyury* expression also from WT cells in gastruloids with high
229 contribution of *Bra*$^{-/-}$ cells suggests cell non-autonomous effects of *Bra*$^{-/-}$ cells. These
230 are most likely explained by disturbances of the previously described feed-forward
231 regulation of *Wnt3a* and *Brachyury* in the tail-bud region (Arnold et al., 2000; Dunty et
232 al., 2008; Martin and Kimelman, 2008; Turner et al., 2014; Yamaguchi et al., 1999). To
233 test this, we performed *in situ* hybridization to analyse expression of *Wnt3a* and the
234 putative *Brachyury* target gene and Wnt co-ligand *Rspo3 (*Koch *et al*., 2017*)* in WT
235 gastruloids, in gastruloids entirely composed of *Bra*$^{-/-}$ cells, and in mixed gastruloids

236 with 80% and 50% *Bra*$^{-/-}$ cell contribution at 72, 96 and 120 h (Fig. 3E). This analysis
237 demonstrates *Brachyury*-requirements for the sustained expression of *Wnt3a*, which
238 is absent from *Bra*$^{-/-}$ gastruloids at 96 h and greatly reduced and mislocalised in mixed
239 gastruloids at 120 h. Interestingly *Wnt3a* expression, which normally is confined to the
240 posterior pole, is found at intermediate levels of mixed gastruloids, most likely resulting
241 from unequal cell distribution of WT and *Bra*$^{-/-}$ cells, which accumulate at the posterior
242 of mixed *Bra*$^{-/-}$: WT gastruloids (see also Fig. 4 and discussion below). Analysis of
243 *Rspo3* expression recapitulates the lack of *Brachyury* expression in *Bra*$^{-/-}$ gastruloids
244 and the prematurely exhausted *Brachyury* expression in *Bra*$^{-/-}$: WT mixed gastruloids
245 (Fig. 3C-E).
246 Next, in addition to the tissue-wide, partially cell non-autonomous phenotype of
247 *Brachyury*-deficiency in gastruloids with a high contribution of *Bra*$^{-/-}$ cells, we analysed
248 the cell-autonomous effects of *Brachyury*-deficiency in conditions with low contribution
249 of mutant cells (Fig. 4). We generated chimeric gastruloids by mixing cells in a 10:90
250 ratio of *Bra*$^{-/-}$: WT mESCs (Fig. 4A, B) and compared resulting gastruloids with controls
251 where 10% mT-labelled WT cells were used (Fig. 4C, D). Further controls were
252 included where cells were mixed at 50:50 ratios (Supplementary Fig. 4A, B). WT cells
253 randomly disperse, while *Bra*$^{-/-}$ exhibit a tissue sorting behaviour (Fig. 4A-D,
254 Supplementary Fig. 4A, B). At 120 h of culture *Bra*$^{-/-}$ cells are predominantly found
255 along the midline in the interior of the gastruloids, and in the posterior pole (Fig. 4B).
256 To determine tissue identity of these regions we used immunofluorescence (IF)
257 staining against FOXA2 and CDH1 (E-Cadherin), labelling DE (Viotti et al., 2014),
258 SOX2 labelling neural tube progenitors (Wood and Episkopou, 1999), and FOXC2 as
259 mesoderm marker, and combined IF-staining with the fluorescent labels of WT (mG)
260 and *Bra*$^{-/-}$ cells (mT) (Fig. 4E-I). FOXA2 and CDH1 stainings indicate that *Bra*$^{-/-}$ cells
261 are biased towards DE and favored to form the gut tube-like structure in the midline of
262 gastruloids (Fig. 4E, G, H). This finding not only demonstrates that *Brachyury* is
263 dispensable for DE lineage specification from pluripotent cells, but suggests that
264 *Brachyury* actually counteracts DE specification programs and thus may not represent
265 a suitable marker for early DE-forming cells as previously suggested (Kubo et al.,
266 2004). In addition to their contribution to endoderm structures of chimeric gastruloids,
267 *Bra*$^{-/-}$ cells are predominantly found in the posterior region of chimeric gastruloids.
268 Here, *Bra*$^{-/-}$ cells show SOX2 staining marking them as neural tube progenitors (Fig.
269 4F, G). Furthermore, *Bra*$^{-/-}$ cells are rather excluded from the FOXC2-positive

270 mesoderm forming domain (Fig. 4I), in accordance with previous findings about NE-
271 repressive and mesoderm promoting functions of *Brachyury* (Koch et al., 2017; Tosic
272 et al., 2019).
273 In conclusion, this study illustrates the feasibility and experimental potency to use
274 functional genetics in mESCs to generate chimeric 3D-gastruloids. These allow for the
275 rapid and reproducible analysis of gain- and loss-of-gene functions, which may reveal
276 different phenotypic outcomes according to the degree of cellular contribution in
277 chimeric gastruloids. Close attention should be paid to control for the general variability
278 in mESC morphogenetic and differentiation behaviour, which might not strictly depend
279 on the genetic manipulation of each cell line. We did not experience these problems in
280 presented experiments, as they were all based on usage of mESCs lines originating
281 from the same parental clone (A2lox, Iacovino et al., 2014).
282 Here, we used the inducible expression of the Tbx transcription factor *Eomes* to
283 demonstrate how limitations of 3D gastruloids can be overcome by genetically
284 providing regulatory cues that are missing or underrepresented in CHIR-only treated
285 gastruloids, namely the induced formation of anterior mesoderm derivatives including
286 heart tissue. The analysis of *Brachyury*-deficient cells in chimeric gastruloids
287 remarkably reflects aspects previous studies of embryonic chimeras (Wilson et al.,
288 1993; Wilson et al., 1995; Wilson and Beddington, 1997). Here, *Bra*$^{-/-}$ cells
289 progressively accumulate in the tailbud region, most likely as result of *Brachyury*
290 functions in regulation of mesoderm cell migration leading to passive replacement of
291 mutant cells into the most posterior embryonic regions (Wilson et al., 1995; Wilson and
292 Beddington, 1997). It thus will be interesting to follow morphogenetic cell movements
293 of *Bra*$^{-/-}$ cells in chimeric gastruloids. In addition, the analysis of *Brachyury* deficient
294 cells in chimeras with low cell contribution showed a cell-autonomous bias towards the
295 DE, a cell lineage that strictly depends on *Eomes* functions (Arnold et al., 2008; Teo et
296 al., 2011). Since *Brachyury* and *Eomes* are co-expressed in cells of the early primitive
297 streak in early gastrulating embryos (Tosic et al., 2019), this poses the interesting
298 question about reciprocal regulatory interactions between these two related Tbx
299 factors.
300 In summary, this study demonstrates that chimeric gastruloids represent a powerful
301 experimental tool for the analysis of gastrulation stage embryogenesis. Gastruloids
302 already exhibit a high degree of experimental accessibility, observability and
303 scalability. The additional implementation of chimeric gastruloids allows to analyse

304 gene-functions at cellular level without affecting the general gastruloid architecture and
305 might thus enhance our understanding of cell-signal interactions during gastrulation
306 morphogenesis.
307
308 **Materials and Methods**
309 **Cell lines**
310 A2lox mESCs (Iacovino et al., 2014) were cultured in Dulbecco's modified Eagle's
311 medium (DMEM) containing 15 % fetal bovine serum (FBS, Gibco), 2 mM L-glutamine,
312 1X non-essential amino acids (NEAA), 1 mM sodium-pyruvate, 1X
313 penicillin/streptomycin (all from Gibco), 100 µM β-mercaptoethanol (Sigma), Leukemia
314 inhibitory factor (ESGRO LIF, Merck Millipore, 1000 U/ml), and 2i: CHIR99021 (Axon
315 Medchem, 3 µM) and PD0325901 (Axon Medchem, 1 µM) on 0.1% gelatine-coated
316 dishes. The medium was changed daily and mESCs were passaged every other day.
317 The generation of homozygous *Bra*$^{-/-}$ mESCs and of A2lox mESCs harbouring
318 monoallelic dox- inducible expression cassette for *Eomes*.GFP were described
319 previously (Tosic et al., 2019). A2lox cells with membrane-tagged fluorescent labels
320 (membrane-Tomato, mT, and membrane-GFP, mG) were generated by targeted
321 integration of a mT/mG targeting vector (Muzumdar et al., 2007), Addgene plasmid
322 #17787) into the Rosa26 locus. 1x10^{6} A2lox mESCs (WT and *Bra*$^{-/-}$) were transfected
323 with 2.5 µg of linearized vector using the Nucleofector ESC kit (Lonza) and G418
324 selected (350 µg/ml) on a monolayer of MitoC (Sigma)-mitotically inactivated STO
325 feeder cells. mT-expressing ESC clones were picked on day 9 of selection. To convert
326 the expression of the membrane-Tomato (mT) to membrane-GFP (mG) in WT A2lox
327 mESCs, cells were treated for 24 h with 5 µg/ml Doxycyclin (Sigma, D9891) for induced
328 expression of the Cre-recombinase from the Dox-inducible locus of A2lox WT cells to
329 excise the loxP-flanked mT expression cassette and bring the mG expression cassette
330 under the transcriptional control of the Rosa26 gene locus. After Cre-excision mG-
331 expressing WT A2lox mESCs underwent one round of clonal selection by minimal
332 dilution of 500 cells onto a 10 cm cell culture dish.
333
334 **Generation of chimeric gastruloids**
335 Gastruloids were generated using published protocols (van den Brink et al., 2020) with
336 some modifications as outlined below. Gastruloid formation was performed in ESGRO
337 Complete Basal Medium (Merck Millipore) in the absence of Matrigel. To generate

338 chimeric gastruloids using different mESCs by merging of preformed aggregates 150
339 cells of each ESC line were aggregated in 40 µl of ESGRO basal medium in 96-well
340 format (Greiner ultra-low attachment plates, No. 650970) for 24 h before merging by
341 combining two aggregates into the same well. At 48 h following first aggregate
342 formation, fused gastruloids were induced by administration of 3 µM CHIR and if
343 indicated with doxycycline (1 µg/µl, Sigma) for 24 h. In the course of gastruloid culture,
344 the medium was changed daily at 72, 96, 120 and 144 h. For the generation of
345 gastruloids by mixing of different ESC lines, aggregates were formed from a total of
346 300 mESCs at various ratios between the two ESC lines, and further gastruloid
347 formation followed by previously used protocols (van den Brink et al., 2020).
348
349 **Whole mount *in situ* hybridization**
350 Whole-mount *in situ* hybridization was performed according to standard protocols
351 using standard probes for *Mlc2a, Nkx2.5*, *Wnt3a*, and *Rspo3* (Details can be requested
352 from the authors). In brief, gastruloids were fixed in 4% PFA/PBS o/n at 4°C,
353 dehydrated via a methanol series and stored in methanol at -20°C. After rehydration
354 gastruloids were bleached in 6 % H_2O_2 for 5 min, digested by 1.6 µg/ml ProteinaseK
355 in PBT for 2 min, and postfixed in 4% PFA/0,2% glutaraldehyde for 20 min before
356 prehybridization for 2 h and hybridization o/n according to standard protocols. DIG-
357 labelled RNA probe was detected using anti-Digoxigenin-AP Fab fragments (Roche)
358 in 1% sheep serum, 2% BBR in MAB (0.1 M Maleic acid, 0.3 M NaCl, NaOH, 1%
359 Tween-20 in H_2O, pH 7.5) and incubation at 4°C o/n. Antibody was washed out by
360 extensive washes in MAB (>24 h, RT), and color reaction performed in BM purple
361 staining solution (Roche) for 2-6 h at RT.
362
363 **Whole mount immunofluorescence staining**
364 Gastruloids were fixed in 4% PFA /PBS for 1 h at 4°C, permeabilized (0.3% Triton X-
365 100/ PBT, 30 min) and blocked in 1% BSA / PBT for 1h at RT. Primary antibody
366 incubation was performed at 4°C o/n in 1% BSA / PBT, gastruloids washed 4x in PBT
367 before secondary fluorescence-conjugated antibody incubation for 3 h followed by
368 DAPI staining for 30 min at RT. Primary antibodies used were BRACHYURY (R&D
369 Systems; AF2085), CDX2 (Biogenex; MU392A) FOXA2 (Cell Signaling; 8186S), E-
370 Cadherin (BD Transduction Laboratories; 610182), SOX2 (R&D Systems; AF2018),
371 FOXC2 (R&D Systems; AF6989) at suggested dilutions. Secondary anti-goat, anti-

372 rabbit, anti-mouse and anti-sheep Alexa Fluor 647-conjugated antibodies (Thermo
373 Fisher), and anti-goat CF405M (Biotium).
374
375 **Histological sections of gastruloids**
376 Fixed gastruloids were processed through 15% and 30% sucrose/PBS and incubated
377 for at least 1h in embedding medium (15% sucrose, 7,5% gelatin in PBS) before cryo-
378 embedding. Embedded gastruloids were cut with into 8 µm sections, mounted with
379 ProLong Diamond Antifade Mountant (Life Technologies, P36970) and imaged as
380 described below.
381
382 **Imaging**
383 Images were acquired on a Leica DMi8 Thunder Imager System or a Leica M165FC
384 Stereo microscope. Images were processed in the Leica LASX software and Affinity
385 Photo. During time lapse imaging gastruloids were maintained under constant
386 conditions at 37°C, 5% CO_2.
387
388 **Data acquisition and statistics**
389 The percentage of beating gastruloids (Fig. 2D) was determined by manually counting
390 during life imaging in three individual experiments. Following numbers of gastruloids
391 were evaluated: 23 (+DOX) and 21 (-DOX) for n1; 61(+DOX) and 57 (-DOX) for n2,
392 and 91(+DOX) and 90 (-DOX) for n3.
393 The length of the anterior-posterior axis of gastruloids (Fig. 2J) was measured using
394 the LASX software (Leica) for n=34 (WTmG-WTmT) and n=36 (WTmG-TRE.*Eo*mT).
395 Graphs (Scatter plot; Mean with SD) and column statistics were acquired with the
396 GraphPad Prism software (Version 5.04).
397
398 **Acknowledgements**
399 We thank T. Bass for excellent technical assistance and Michael Kyba for the A2lox
400 ESC line.
401
402 **Funding**
403 This work was supported by the German Research Foundation (DFG) through the
404 Heisenberg Program (AR 732/3-1), project grant (AR 732/2-1,) project B07 of SFB
405 1140 (project ID 246781735), project A03 of SFB 850 (project ID 89986987), project

P7 of SFB 1453 (project ID 431984000), and Germany's Excellence Strategy (CIBSS – EXC-2189 – Project ID 390939984) to S.J.A., and by the MOTI-VATE program of the Freiburg Medical Faculty supported by the Else-Kröner-Fresenius-Stiftung to A.C.

Competing interests

The authors declare no competing interests.

Author contributions

A.E.W., K.M.S., A.C., C.M.S. generated different ESC lines and performed experiments. A.E.W, S.P. and S.J.A. planned and analysed experiments. A.E.W. and S.J.A. prepared figures, wrote and edited the manuscript with input from all authors. S.J.A. conceived the study.

References

Amadei, G., Lau, K. Y. C., De Jonghe, J., Gantner, C. W., Sozen, B., Chan, C., Zhu, M., Kyprianou, C., Hollfelder, F. and Zernicka-Goetz, M. (2021). Inducible Stem-Cell-Derived Embryos Capture Mouse Morphogenetic Events In Vitro. *Dev Cell* **56**, 366-382 e369.

Arnold, S. J., Hofmann, U. K., Bikoff, E. K. and Robertson, E. J. (2008). Pivotal roles for eomesodermin during axis formation, epithelium-to-mesenchyme transition and endoderm specification in the mouse. *Development* **135**, 501-511.

Arnold, S. J. and Robertson, E. J. (2009). Making a commitment: cell lineage allocation and axis patterning in the early mouse embryo. *Nat Rev Mol Cell Biol* **10**, 91-103.

Arnold, S. J., Stappert, J., Bauer, A., Kispert, A., Herrmann, B. G. and Kemler, R. (2000). Brachyury is a target gene of the Wnt/beta-catenin signaling pathway. *Mech Dev* **91**, 249-258.

Beccari, L., Moris, N., Girgin, M., Turner, D. A., Baillie-Johnson, P., Cossy, A. C., Lutolf, M. P., Duboule, D. and Arias, A. M. (2018). Multi-axial self-organization properties of mouse embryonic stem cells into gastruloids. *Nature* **562**, 272-276.

Costello, I., Pimeisl, I. M., Drager, S., Bikoff, E. K., Robertson, E. J. and Arnold, S. J. (2011). The T-box transcription factor Eomesodermin acts upstream of Mesp1 to specify cardiac mesoderm during mouse gastrulation. *Nat Cell Biol* **13**, 1084-1091.

Dunty, W. C., Jr., Biris, K. K., Chalamalasetty, R. B., Taketo, M. M., Lewandoski, M. and Yamaguchi, T. P. (2008). Wnt3a/beta-catenin signaling controls posterior body development by coordinating mesoderm formation and segmentation. *Development* **135**, 85-94.

Halpern, M. E., Ho, R. K., Walker, C. and Kimmel, C. B. (1993). Induction of muscle pioneers and floor plate is distinguished by the zebrafish no tail mutation. *Cell* **75**, 99-111.

Harrison, S. E., Sozen, B., Christodoulou, N., Kyprianou, C. and Zernicka-Goetz, M. (2017). Assembly of embryonic and extraembryonic stem cells to mimic embryogenesis in vitro. *Science* **356**.

Harrison, S. E., Sozen, B. and Zernicka-Goetz, M. (2018). In vitro generation of mouse polarized embryo-like structures from embryonic and trophoblast stem cells. *Nat Protoc* **13**, 1586-1602.

Iacovino, M., Roth, M. E. and Kyba, M. (2014). Rapid genetic modification of mouse embryonic stem cells by Inducible Cassette Exchange recombination. *Methods Mol Biol* **1101**, 339-351.

Inman, K. E. and Downs, K. M. (2006). Brachyury is required for elongation and vasculogenesis in the murine allantois. *Development* **133**, 2947-2959.

Kagawa, H., Javali, A., Khoei, H. H., Sommer, T. M., Sestini, G., Novatchkova, M., Scholte Op Reimer, Y., Castel, G., Bruneau, A., Maenhoudt, N., et al. (2022). Human blastoids model blastocyst development and implantation. *Nature* **601**, 600-605.

Koch, F., Scholze, M., Wittler, L., Schifferl, D., Sudheer, S., Grote, P., Timmermann, B., Macura, K. and Herrmann, B. G. (2017). Antagonistic Activities of Sox2 and Brachyury Control the Fate Choice of Neuro-Mesodermal Progenitors. *Dev Cell* **42**, 514-526 e517.

Kubo, A., Shinozaki, K., Shannon, J. M., Kouskoff, V., Kennedy, M., Woo, S., Fehling, H. J. and Keller, G. (2004). Development of definitive endoderm from embryonic stem cells in culture. *Development* **131**, 1651-1662.

Li, R., Zhong, C., Yu, Y., Liu, H., Sakurai, M., Yu, L., Min, Z., Shi, L., Wei, Y., Takahashi, Y., et al. (2019). Generation of Blastocyst-like Structures from Mouse Embryonic and Adult Cell Cultures. *Cell* **179**, 687-702 e618.

Martin, B. L. and Kimelman, D. (2008). Regulation of canonical Wnt signaling by Brachyury is essential for posterior mesoderm formation. *Dev Cell* **15**, 121-133.

Moris, N., Anlas, K., van den Brink, S. C., Alemany, A., Schroder, J., Ghimire, S., Balayo, T., van Oudenaarden, A. and Martinez Arias, A. (2020). An in vitro model of early anteroposterior organization during human development. *Nature* **582**, 410-415.

Muzumdar, M. D., Tasic, B., Miyamichi, K., Li, L. and Luo, L. (2007). A global double-fluorescent Cre reporter mouse. *Genesis* **45**, 593-605.

Probst, S., Sagar, Tosic, J., Schwan, C., Grun, D. and Arnold, S. J. (2021). Spatiotemporal sequence of mesoderm and endoderm lineage segregation during mouse gastrulation. *Development* **148**.

Rivera-Perez, J. A. and Magnuson, T. (2005). Primitive streak formation in mice is preceded by localized activation of Brachyury and Wnt3. *Dev Biol* **288**, 363-371.

479 **Rossi, G., Broguiere, N., Miyamoto, M., Boni, A., Guiet, R., Girgin, M., Kelly, R. G., Kwon,**
480 **C. and Lutolf, M. P.** (2021). Capturing Cardiogenesis in Gastruloids. *Cell Stem Cell* **28**,
481 230-240 e236.
482 **Teo, A. K., Arnold, S. J., Trotter, M. W., Brown, S., Ang, L. T., Chng, Z., Robertson, E. J.,**
483 **Dunn, N. R. and Vallier, L.** (2011). Pluripotency factors regulate definitive endoderm
484 specification through eomesodermin. *Genes Dev* **25**, 238-250.
485 **Tosic, J., Kim, G. J., Pavlovic, M., Schroder, C. M., Mersiowsky, S. L., Barg, M., Hofherr,**
486 **A., Probst, S., Kottgen, M., Hein, L., et al.** (2019). Eomes and Brachyury control
487 pluripotency exit and germ-layer segregation by changing the chromatin state. *Nat Cell*
488 *Biol* **21**, 1518-1531.
489 **Turner, D. A., Girgin, M., Alonso-Crisostomo, L., Trivedi, V., Baillie-Johnson, P.,**
490 **Glodowski, C. R., Hayward, P. C., Collignon, J., Gustavsen, C., Serup, P., et al.**
491 (2017). Anteroposterior polarity and elongation in the absence of extra-embryonic tissues
492 and of spatially localised signalling in gastruloids: mammalian embryonic organoids.
493 *Development* **144**, 3894-3906.
494 **Turner, D. A., Rue, P., Mackenzie, J. P., Davies, E. and Martinez Arias, A.** (2014).
495 Brachyury cooperates with Wnt/beta-catenin signalling to elicit primitive-streak-like
496 behaviour in differentiating mouse embryonic stem cells. *BMC Biol* **12**, 63.
497 **van den Brink, S. C., Alemany, A., van Batenburg, V., Moris, N., Blotenburg, M., Vivie, J.,**
498 **Baillie-Johnson, P., Nichols, J., Sonnen, K. F., Martinez Arias, A., et al.** (2020). Single-
499 cell and spatial transcriptomics reveal somitogenesis in gastruloids. *Nature* **582**, 405-409.
500 **van den Brink, S. C., Baillie-Johnson, P., Balayo, T., Hadjantonakis, A. K., Nowotschin,**
501 **S., Turner, D. A. and Martinez Arias, A.** (2014). Symmetry breaking, germ layer
502 specification and axial organisation in aggregates of mouse embryonic stem cells.
503 *Development* **141**, 4231-4242.
504 **van den Brink, S. C. and van Oudenaarden, A.** (2021). 3D gastruloids: a novel frontier in
505 stem cell-based in vitro modeling of mammalian gastrulation. *Trends Cell Biol* **31**, 747-
506 759.
507 **Veenvliet, J. V., Bolondi, A., Kretzmer, H., Haut, L., Scholze-Wittler, M., Schifferl, D.,**
508 **Koch, F., Guignard, L., Kumar, A. S., Pustet, M., et al.** (2020). Mouse embryonic stem
509 cells self-organize into trunk-like structures with neural tube and somites. *Science* **370**.
510 **Veenvliet, J. V., Lenne, P. F., Turner, D. A., Nachman, I. and Trivedi, V.** (2021). Sculpting
511 with stem cells: how models of embryo development take shape. *Development* **148**.
512 **Viotti, M., Nowotschin, S. and Hadjantonakis, A. K.** (2014). SOX17 links gut endoderm
513 morphogenesis and germ layer segregation. *Nat Cell Biol* **16**, 1146-1156.

514 **Wilson, V. and Beddington, R.** (1997). Expression of T protein in the primitive streak is
515 necessary and sufficient for posterior mesoderm movement and somite differentiation.
516 *Dev Biol* **192**, 45-58.
517 **Wilson, V., Manson, L., Skarnes, W. C. and Beddington, R. S.** (1995). The T gene is
518 necessary for normal mesodermal morphogenetic cell movements during gastrulation.
519 *Development* **121**, 877-886.
520 **Wilson, V., Rashbass, P. and Beddington, R. S.** (1993). Chimeric analysis of T (Brachyury)
521 gene function. *Development* **117**, 1321-1331.
522 **Wood, H. B. and Episkopou, V.** (1999). Comparative expression of the mouse Sox1, Sox2
523 and Sox3 genes from pre-gastrulation to early somite stages. *Mech Dev* **86**, 197-201.
524 **Wymeersch, F. J., Wilson, V. and Tsakiridis, A.** (2021). Understanding axial progenitor
525 biology in vivo and in vitro. *Development* **148**.
526 **Xu, P. F., Borges, R. M., Fillatre, J., de Oliveira-Melo, M., Cheng, T., Thisse, B. and Thisse,**
527 **C.** (2021). Construction of a mammalian embryo model from stem cells organized by a
528 morphogen signalling centre. *Nat Commun* **12**, 3277.
529 **Yamaguchi, T. P., Takada, S., Yoshikawa, Y., Wu, N. and McMahon, A. P.** (1999). T
530 (Brachyury) is a direct target of Wnt3a during paraxial mesoderm specification. *Genes*
531 *Dev* **13**, 3185-3190.
532 **Yu, L., Wei, Y., Duan, J., Schmitz, D. A., Sakurai, M., Wang, L., Wang, K., Zhao, S., Hon,**
533 **G. C. and Wu, J.** (2021). Blastocyst-like structures generated from human pluripotent
534 stem cells. *Nature* **591**, 620-626.

535

536 **FIGURE LEGENDS**

537 **Fig. 1. Experimental approaches for the generation of chimeric gastruloids**

538 **(A)** Schematic of two alternative experimental approaches to generate chimeric
539 gastruloids from fluorescently labelled embryonic stem cells (mESCs). Wildtype (WT)
540 mESCs are marked by membrane-GFP (mG) and combined with membrane-Tomato
541 (mT) labelled, genetically modified mESCs. The genetic modifications of mESCs
542 comprise homozygous gene deletions (*GeneX*) or inducible gene-expression by the
543 targeting of cDNAs into a fully controllable pre-engineered locus containing a
544 Tetracycline responsive element (TRE) for dox-dependent induction of gene
545 expression (*GeneY*). Chimeric gastruloids are generated by either mixing of mESCs
546 at the beginning of gastruloid culture, or by merging preformed mESCs aggregates
547 preceeding the induction of gastruloids by CHIR. Chimeric gastruloids can be used as
548 versatile novel model system for various types of studies and embryonic research
549 questions as indicated exemplary.

550 **(B)** Schematic of the protocol to form chimeric gastruloids indicating timepoints for
551 either mixing of cells, or merging of aggregates to create chimeric gastruloids.
552 **(C)** Membrane-GFP (mG) labelling of WT mESCs and membrane-Tomato (mT)
553 labelling for genetically modified mESCs allows for distinguishing different cell types in
554 chimeric gastruloids. Scale bars 10 µm.
555 **(D)** Timelapse-imaging of the merging process of pre-formed ESC aggregates at
556 indicated time points. 150 mG and mT mESCs were aggregated for 24 h before
557 merging them by placing them together in 96-well plates. After 1 hr two aggregates
558 spontaneously aggregated and formed stable contacts. Scale bars 100 µm. Also see
559 **Supplementary Movie 1** for a 12 h time-lapse movie.
560 **(E)** Examples of mixed ESC aggregates at 24 h after aggregation of 300 mESCs by
561 mixing mG WT mESCs and mT *Bra*$^{-/-}$ mESCs at indicated ratios. Scale bars 100 µm.
562
563 **Fig. 2. Instructive functions of *Eomes* for cardiac lineage specification in merged**
564 **chimeric gastruloids.**
565 **(A)** Schematic illustrating the generation and culture of chimeric gastruloids by merging
566 preformed aggregates of mG-labelled WT mESCs and mT-labelled mESCs harbouring
567 *EomesGFP* in the Doxycycline (Dox)-inducible gene locus (TRE.*EomesGFP, short*
568 TRE.*Eo*).
569 **(B)** Fluorescent microscopy of TRE.*Eo* mESCs showing nuclear expression of
570 doxycycline-induced (+DOX) EOMES.GFP after 24 h of administration that is absent
571 in -DOX conditions. Scale bars 10 µm.
572 **(C)** Brightfield (left) and fluorescent (right) images of a chimeric gastruloid at 168 h
573 following induced *Eomes* expression showing the region of beating cardiomyocytes
574 within the gastruloid that is mostly derived of mT-labelled TRE.*Eo* cells. The dashed
575 line indicates the domain of beating cells. See also **Supplementary Movie 2** for the
576 corresponding time-lapse movie.
577 **(D)** Statistics comparing the percentage of beating gastruloids at 168 h in gastruloids
578 with forced *Eomes* expression +DOX (33.7% ± 3.0) and uninduced controls -DOX
579 (1.5% ± 2.5) in n=3 independent experiments that are colour-encoded in orange, blue,
580 and purple. Error bars indicate SD.
581 **(E, F)** Fluorescent microscopy (left) and whole-mount *in situ* hybridization (right) of the
582 same chimeric gastruloids following induced *Eomes*-expression (+DOX) showing

583 instructive functions of forced *Eomes*-expression in TRE.*Eo* cells for the induction of
584 cardiac progenitors, marked by expression of (**E**) *Mlc2a* (n=12), and (**F**) *Nkx2.5* (n=10).
585 **(G, H)** Fluorescent microscopy (left) and immunofluorescence staining (right) showing
586 positioning of TRE.*Eo* cells at the opposite pole of posterior **(G)** BRACHYURY (a-BRA)
587 (n=24) and **(H)** CDX2 (n=10) expression. Scale bars 100 µm in C, E-H.
588
589 **Fig. 3. *Brachyury* functions during axis-elongation in chimeric gastruloids**
590 **generated by cell mixing with high *Bra*$^{-/-}$ cell contribution.**
591 **(A)** Schematic illustrating the generation of chimeric gastruloids by mixing of mG-
592 labelled WT mESCs and mT-labelled Brachyury-deficient (*Bra*$^{-/-}$) mESCs.
593 **(B)** Chimeric gastruloids at 120 h generated by mixing of *Bra*$^{-/-}$ (mT) and WT (mG)
594 mESCs at indicated ratios of cell numbers. Gastruloids with a contribution of *Bra*$^{-/-}$ cells
595 above 80 % show reduced axial elongation. Gastruloids entirely generated from *Bra*$^{-/-}$
596 cells fail to axially extend beyond an oval shape. At WT (mG) cell contribution > 50 %
597 axial elongation is similar to WT gastruloids but occasionally shows a thinning of the
598 posterior portion. Across all experiments *Bra*$^{-/-}$ (mT) cells preferentially contribute to the
599 posterior portion of mixed gastruloids. Anterior is oriented to the top and posterior to
600 the bottom in all images.
601 **(C, D)** Immunofluorescence staining against BRACHYURY (a-BRA) in gastruloids
602 generated by cell mixing of *Bra*$^{-/-}$ and WT cells in ratios of 80:20 (**C**) and 50:50 (**D**) at
603 indicated timepoints, showing less confined and reduced BRACHYURY expression in
604 80:20 chimeras at 96 and 120 h in comparison to posteriorly localized, robust
605 BRACHYURY expression in 50:50 chimeras. Images are representatives of n=14 (72
606 h); n=9 (96 h); n=14 (120 h) in (**C**), and n=16 (72 h); n=25 (96 h), n=18 (120 h)
607 gastruloids in (**D**).
608 **(E)** Whole-mount *in situ* hybridization for *Wnt3a* and *Rspo3* of WT, Bra$^{-/-}$-null and
609 chimeric gastruloids of indicated cell ratios at 72 h, 96 h, and 120 h showing
610 mislocalised and reduced expression of *Wnt3a* and *Rspo3* in Bra-deficient and
611 chimeric WT: Bra$^{-/-}$ mixed gastruloids. The frequencies of representative staining
612 pattern per numbers of examined gastruloid are indicated below each image. Scale
613 bars 100 µm in B-D.
614
615 **Fig. 4. Brachyury functions for cell lineage specification and tissue sorting in**
616 **chimeric gastruloids with low *Bra*$^{-/-}$ cell contribution.**

617 **(A-D)** Chimeric gastruloids generated by mixing of 10% *Bra*$^{-/-}$ (mT) and 90 % WT (mG)
618 ESCs at **(A)** 72 h and 96 h**,** and **(B)** three representative gastruloids at 120 h showing
619 the spectrum of distribution of *Bra*$^{-/-}$ cells between the posterior pole and the midline of
620 chimeric gastruloids.
621 (**C, D**) Control chimeric gastruloids generated by mixing of 10% WT (mT) and 90% WT
622 (mG) ESCs at **(C)** 72 h, 96 h, and **(D)** three replicates at 120 h don't show distinct
623 patterns of cell distribution.
624 **(E-G)** Immunofluorescence staining against (**E**) FOXA2 (n=6) and (**F**) SOX2 (n=8)
625 individually, and **(G)** double IF staining showing the tissue contribution of *Bra*$^{-/-}$ cells to
626 FOXA2+ endoderm and SOX2+ posterior cells (n=14).
627 (**H**) *Bra*$^{-/-}$ cells contribute to the forming primitive gut tubes (arrows) and are positive for
628 the epithelial marker CDH1 (E-Cadherin) (n=3).
629 **(I)** *Bra*$^{-/-}$ cells are mostly excluded from a mesodermal domain that is positive for
630 FOXC2 (n=7). Scale bars 100 µm.
631
632

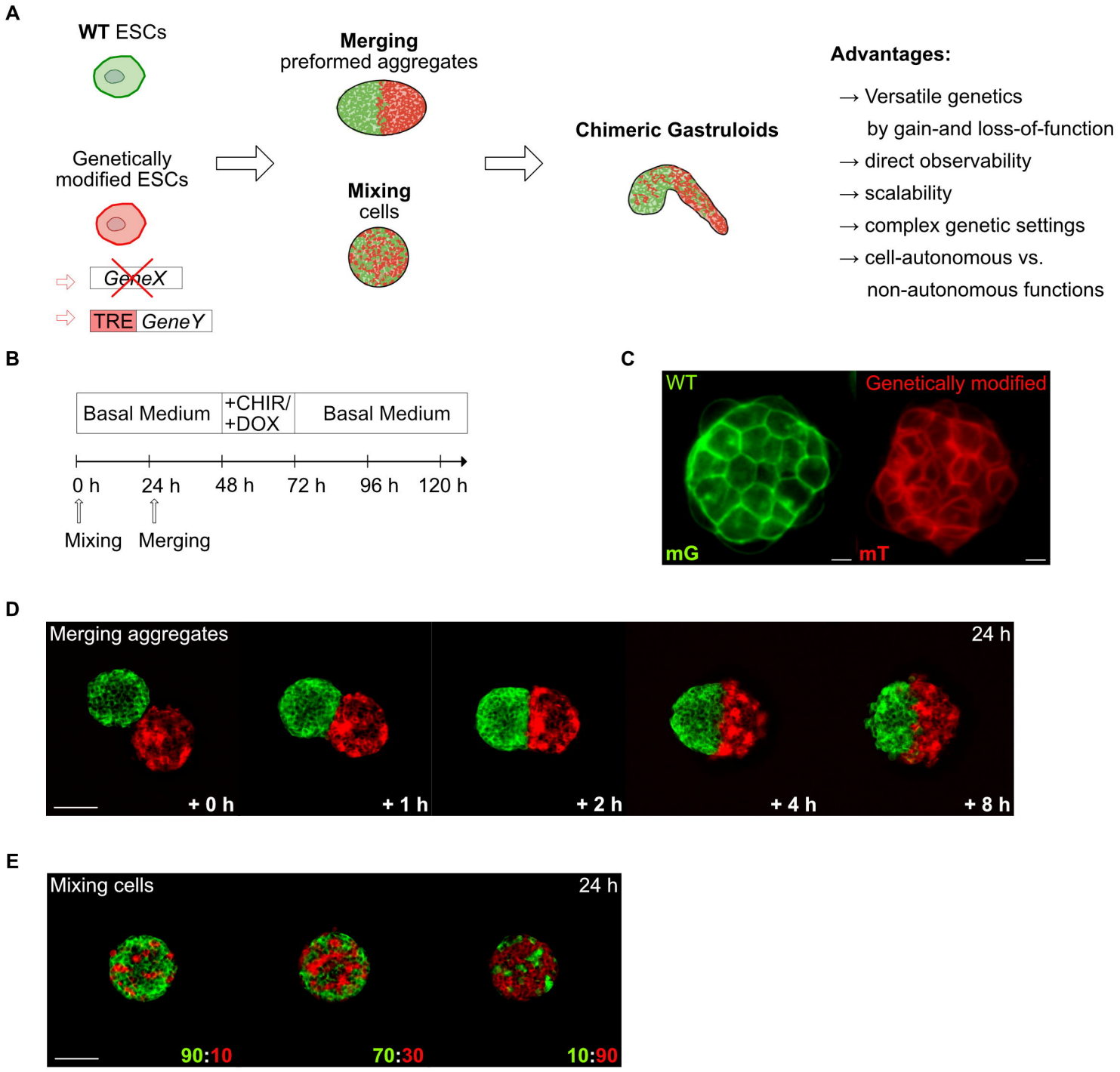
A
WT ESCs
Genetically modified ESCs
GeneX
TRE GeneY
Merging
preformed aggregates
Mixing
cells
Chimeric Gastruloids
Advantages:
→ Versatile genetics by gain-and loss-of-function
→ direct observability
→ scalability
→ complex genetic settings
→ cell-autonomous vs. non-autonomous functions
B
Basal Medium
+CHIR/ +DOX
Basal Medium
0 h
24 h
48 h
72 h
96 h
120 h
Mixing
Merging
C
WT
Genetically modified
mG
mT
D
Merging aggregates
24 h
+ 0 h
+ 1 h
+ 2 h
+ 4 h
+ 8 h
E
Mixing cells
24 h
90:10
70:30
10:90

Fig. 1

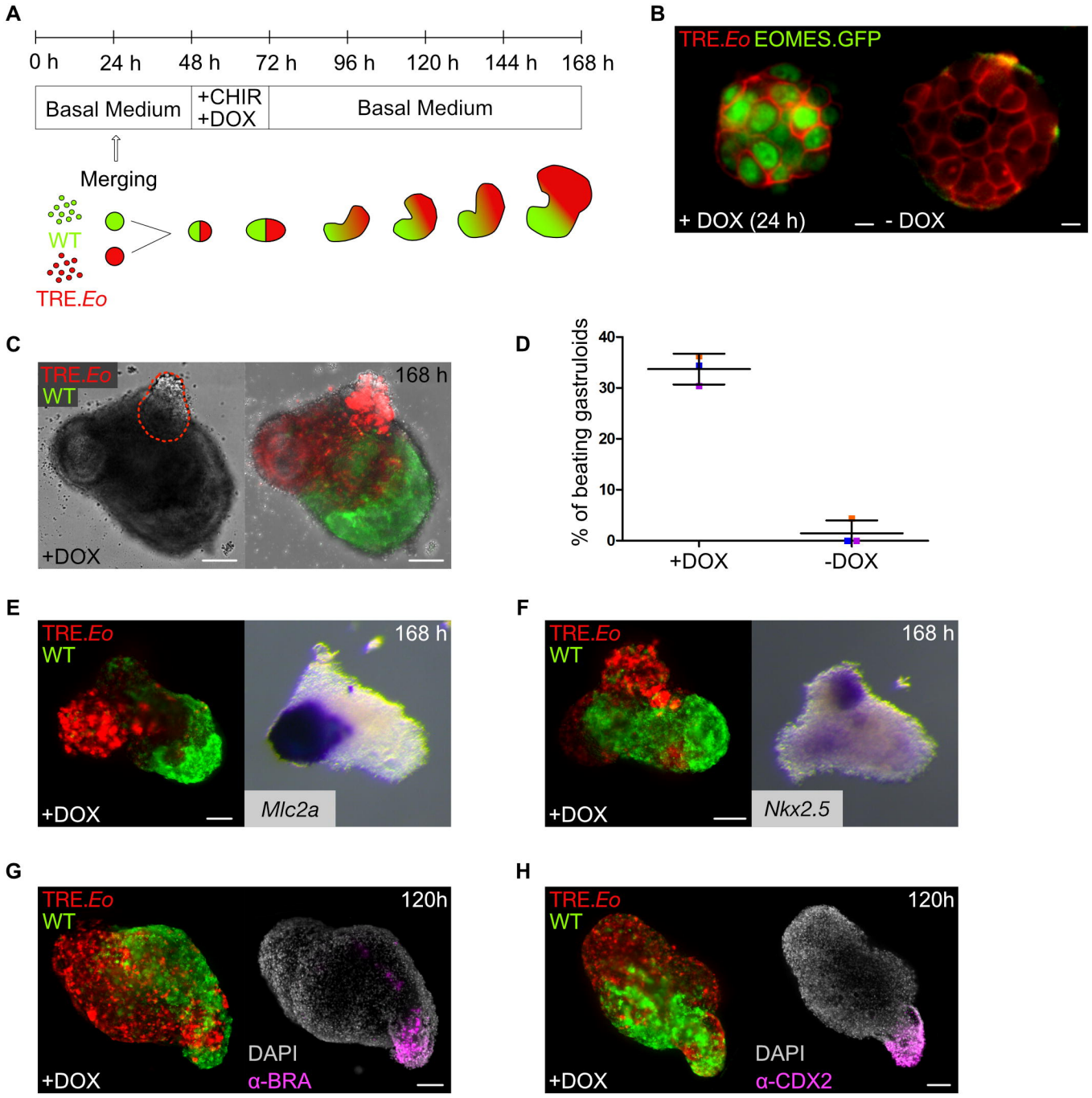
A
0 h
24 h
48 h
72 h
96 h
120 h
144 h
168 h
Basal Medium
+CHIR
+DOX
Basal Medium
Merging
WT
TRE.Eo
B
TRE.Eo EOMES.GFP
+ DOX (24 h)
- DOX
C
TRE.Eo
WT
168 h
+DOX
D
% of beating gastruloids
40
30
20
10
0
+DOX
-DOX
E
TRE.Eo
WT
168 h
+DOX
Mlc2a
F
TRE.Eo
WT
168 h
+DOX
Nkx2.5
G
TRE.Eo
WT
120h
DAPI
α-BRA
+DOX
H
TRE.Eo
WT
120h
DAPI
α-CDX2
+DOX

Fig. 2

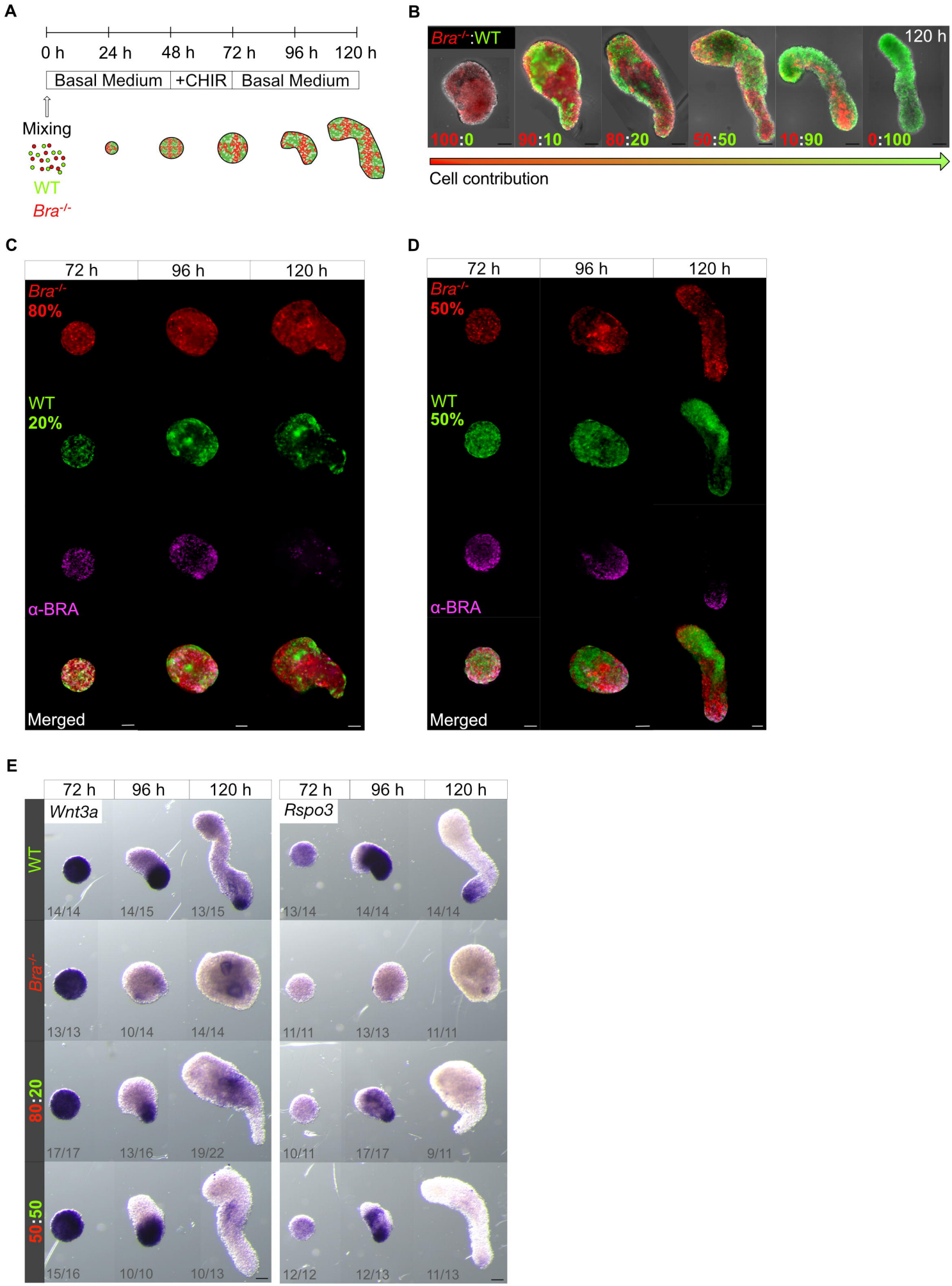
A
0 h
24 h
48 h
72 h
96 h
120 h
Basal Medium
+CHIR
Basal Medium
Mixing
WT
Bra-/-
B
Bra-/-:WT
120 h
100:0
90:10
80:20
50:50
10:90
0:100
Cell contribution
C
72 h
96 h
120 h
Bra-/-
80%
WT
20%
α-BRA
Merged
D
72 h
96 h
120 h
Bra-/-
50%
WT
50%
α-BRA
Merged
E
72 h
96 h
120 h
Wnt3a
Rspo3
WT
Bra-/-
80:20
50:50
14/14
14/15
13/15
13/14
14/14
14/14
13/13
10/14
14/14
11/11
13/13
11/11
17/17
13/16
19/22
10/11
17/17
9/11
15/16
10/10
10/13
12/12
12/13
11/13

Fig. 3

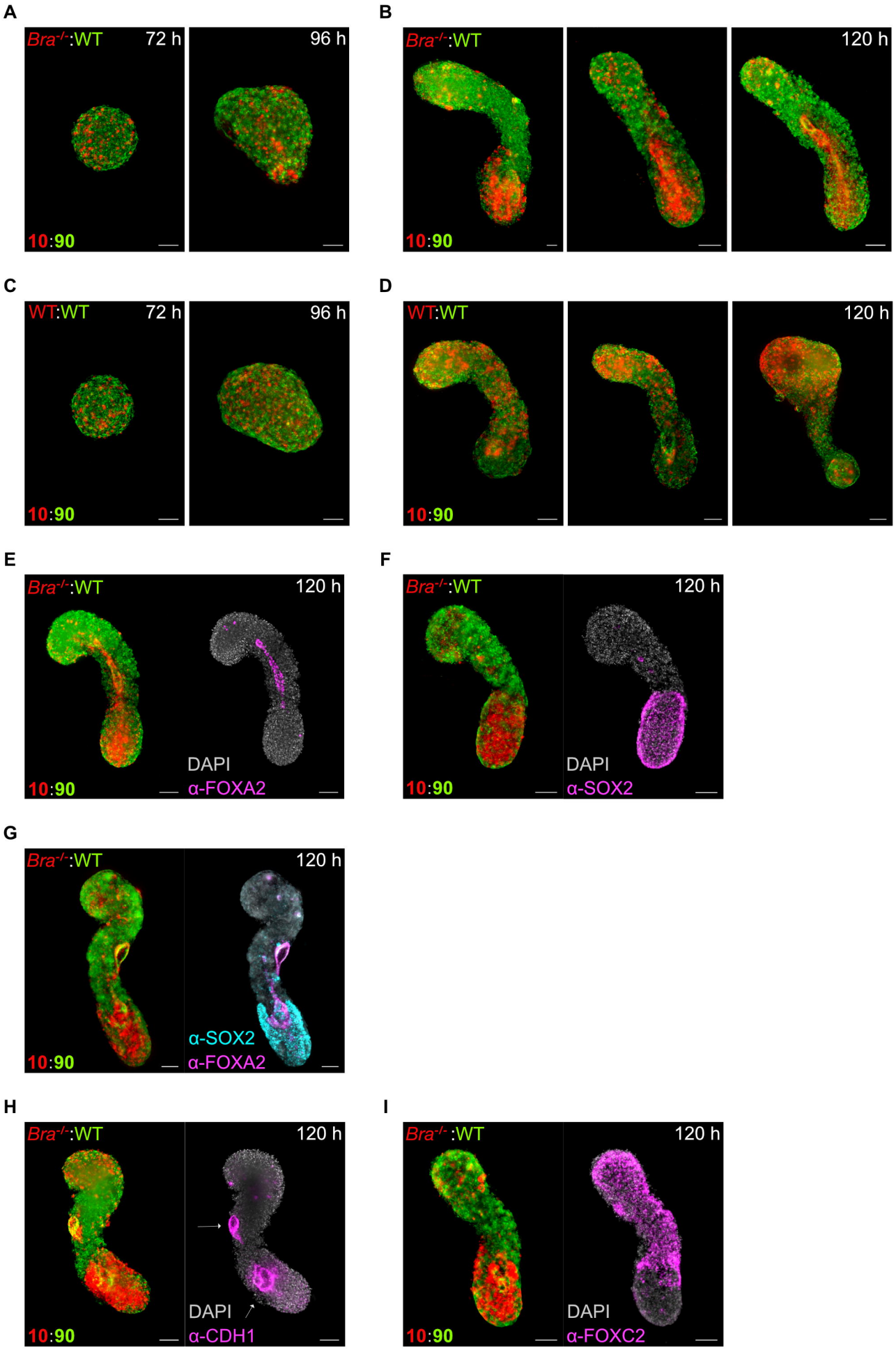
A
Bra-/-:WT
72 h
96 h
10:90
B
Bra-/-:WT
120 h
10:90
C
WT:WT
72 h
96 h
10:90
D
WT:WT
120 h
10:90
E
Bra-/-:WT
120 h
DAPI
α-FOXA2
10:90
F
Bra-/-:WT
120 h
DAPI
α-SOX2
10:90
G
Bra-/-:WT
120 h
α-SOX2
α-FOXA2
10:90
H
Bra-/-:WT
120 h
DAPI
α-CDH1
10:90
I
Bra-/-:WT
120 h
DAPI
α-FOXC2
10:90

Fig. 4